COMMUNICATION

Phase Engineering

ADVANCED
THEORY AND
SIMULATIONS
www.advtheorysimul.com

Controllable Phase Stabilities in Transition Metal Dichalcogenides through Curvature Engineering: First-Principles Calculations and Continuum Prediction

Bin Ouyang,* Pengfei Ou, and Jun Song*

A controllable phase transition between the semiconducting 2H phase and metallic/semimetallic T (1T, 1T′, and 1T″) isomorphs provides an effective route to tune and even switch physical and electronic properties within 2D transition metal dichalcogenides (TMDs). In this study, the feasibility of curvature engineering in manipulating the structural phase is investigated employing first-principles density functional theory (DFT) calculations and continuum mechanics analysis. With WSe$_2$ and MoTe$_2$ as TMD representatives, it is found that bending deformation can not only energetically induce 2H → T (1T, 1T′, or 1T″) phase transformation, but also kinetically facilitate the phase transition by lowering transition activation barriers. Moreover, a phase stability diagram is constructed which suggests ways of achieving both uniformly 2H → T phase transition and programming printing of T phases in 2H-TMD membranes. The theoretical results not only suggest a new feasible experimental design strategy of phase engineering, but also sheds light on novel device design with the patterning of T phases on the 2H-TMD membrane.

The fascinating physical and chemical properties of the atomically thin VI transition metal dichalcogenide (TMD), a material consisting of two layers of chalcogenide atoms sandwiching one layer of VI transition metal atoms in between, has inspired numerous research studies toward ultra-high light absorption and emission,[1] nanoscale piezoelectric behaviors,[2–5] and extraordinary valleytronics effects,[2,6,7] showing great promise in numerous applications, such as solar energy,[8–14] illumination,[11,14–17] nano power generator,[2] and valleytronics devices.[6,7,14]

Recently, the TMD family attracts further attention because of polymorphism. As shown by many studies,[7,18–21] besides the normal octahedral 2H phase, TMDs may assume the form of the trigonal 1T phase or its distorted allotropes (1T′ and 1T″). The divergent properties and polymorphic phases provide an extra technological avenue[22–35] toward tuning of the performance of TMD-based devices. In this regard, precise control of phase transitions in TMDs would be necessary. Recently, there have been several studies[18–21] proposing different ways to engineer phase transitions in TMDs. Intercalation-based method has been widely adapted, it is easily achieved but would introduce defects and impurities into the system.[26,33] Meanwhile, planar strain engineering has been proposed and investigated theoretically since it may offer more controllability and flexibility.[19,20,33,36,37] However, the threshold planar strains for triggering phase transition in TMDs is cloase or larger than the planar elastic limit of TMDs.[19,20] This level of strain is very challenging or even impossible to achieve in experiments.

In this article, we demonstrate curvature engineering as a route to induce phase transition in TMDs. It also provides an alternative other than planar straining to involve strain in engineering phases in TMDs, but with a more feasible strain condition. Employing the nanotube model, the effect of bending deformation in modifying the phase stability and kinetics of phase transition (of H and T phases) in TMDs was systematically examined combining first-principles density functional theory (DFT) calculations and continuum mechanics modeling. A phase stability diagram has been constructed to directly illustrate the dependence of phase preference on bidirectional curvatures, based on which design strategies utilizing curvature engineering can be proposed. Considering the experimental achievability, we have presented a schematic design of rippling and nanoindentation for achieving more flexible phase transitions.

Directly associated with curvature engineering is the introduction of deformation and strain energy. However, accurate prediction of the strain energy in a curved structure is quite challenging in DFT modeling due to the periodic boundary condition and geometric constraint[38–40] in a simulation cell. In the form of a nanotube, the TMD material experiences bending type of deformation with a fixed curvature.[37,39–42] As a result, the nanotube can serve as an idealized atomistic model for examining the bending induced deformation in TMDs.

Dr. B. Ouyang
Department of Materials Science and Engineering
University of California Berkeley
Berkeley, CA 94720, USA
E-mail: bouyang@berkeley.edu

P. Ou, Dr. J. Song
Department of Mining and Materials Engineering
McGill University
Montreal, QC H3A 0C5, Canada
E-mail: jun.song2@mcgill.ca

The ORCID identification number(s) for the author(s) of this article can be found under https://doi.org/10.1002/adts.201800003
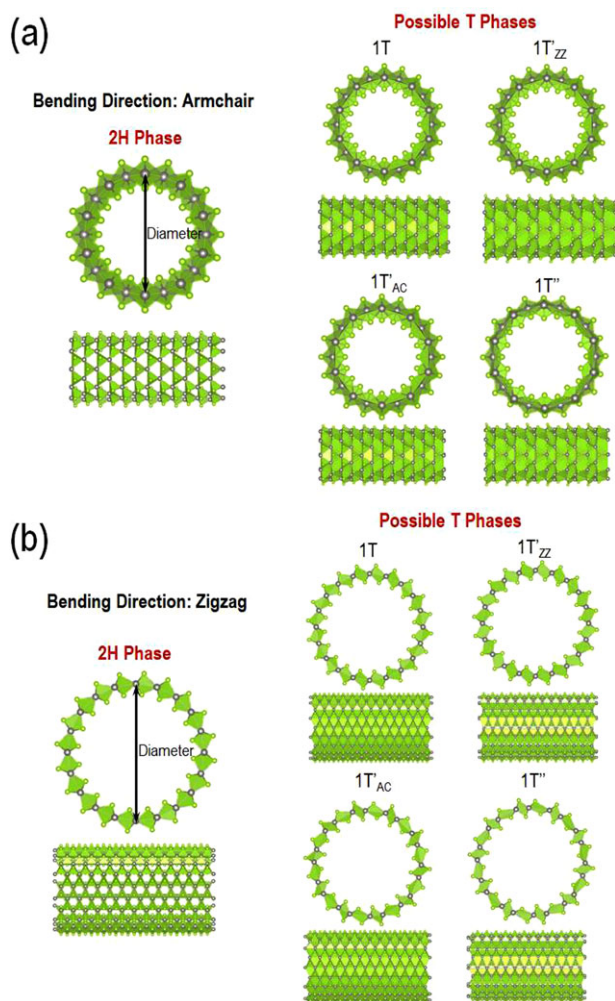
Figure 1. Nanotube models resulted from bending along the a) armchair (AC), and b) zigzag (ZZ) directions. For each bending direction, the 2H phase and the four possible T phases of different Peierls distortions are illustrated. The metal atoms (Mo or W) are colored gray while the chalcogen atoms are colored green.

Two bending directions are considered in our study, that is, bend along armchair direction or zigzag direction, corresponding to nanotube models with $(n,0)$ and (n,n) chirality, respectively. Even though the 1T phase can be directly formed with upper sulfur plane gliding from 2H phase[20,33] it is unstable so that Peierls distortion always takes place,[18–20] which leads to the formation of 1T' or 1T'' phase. Due to the hexagonal structure of TMDs, Peierls distortion can occur in armchair direction, zigzag direction, or both.[18–20] Therefore, as demonstrated in **Figure 1**, for each bending direction considered, there will be four competing T phases existing depending on the direction of Peierls distortion. In addition to the 1T phase, the 1T' phase with Peierls distortion along AC direction is denoted as 1T'$_{AC}$, while 1T'$_{ZZ}$ represents the phase with Peierls distortion occurring at ZZ direction. Additionally, 1T'' phase represents the case in which Peierls distortion takes place in both AC and ZZ directions.

First-principles DFT calculations were then performed using the Vienna Ab Initio Simulation Package (VASP)[43] to exam-

ine the energetics and phase stability of TMD nanotubes. The Perdew–Burke–Ernzserhof (PBE) functional and the projector-augmented wave (PAW)[19,20,43,44] method were used. An energy cutoff of 400 eV and $1 \times 7 \times 1$ k-point grid was applied for each of the calculations. Benchmark calculations were conducted to show that the above energy cutoff and k-point grid yield sufficient accuracy (i.e., energy difference <0.02 eV). The vacuum space between the structure and its image was set as 20 Å to eliminate image interactions. For a TMD nanotube of diameter d and of phase ϕ (2H or T), the associated energy difference with respect to the reference TMD monolayer (normalized by number of MoS_2 units) $E_S^\phi(d)$, can be computed as:

$$E_S^\phi(d) = E_{tube}^\phi(d) - E_{ml}^\phi \tag{1}$$
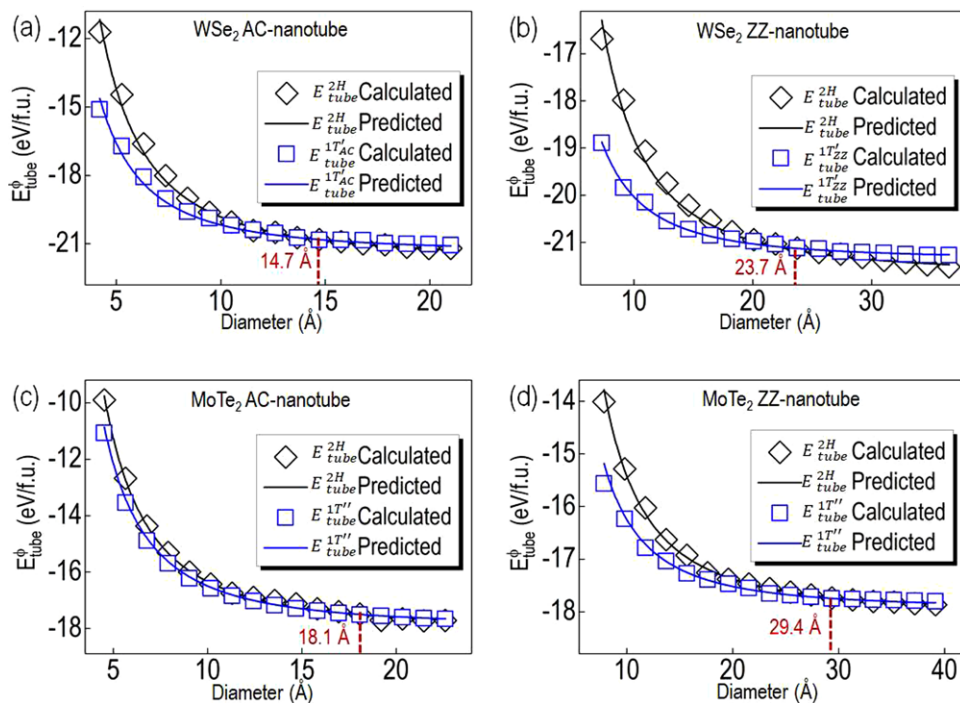
where $E_{tube}^\phi(d)$ and E_{ml}^ϕ, refer to normalized total energy per formula unit (eV f.u.$^{-1}$) of the nanotube of diameter d and the reference TMD monolayer, respectively, with the superscript ϕ indicating the phase that the nanotube or monolayer assumes. $E_S^\phi(d)$ represents the effective strain energy associated with the bending of a monolayer TMD into a nanotube.

In addition to calculations for obtaining energetics information, kinetic calculations were performed to examine the kinetic procedure of phase transition. Employing transition state theory, the climbed image nudged elastic band (ci-NEB) method[45–48] was adopted to compute the minimum reaction paths (MEPs) and associated energy barriers of 2H/T phase transitions.

The evolution of the normalized total energy of a nanotube $E_{tube}^\phi(d)$ as a function of the diameter d is shown in **Figure 2**. In the illustration, only the lowest-energy T-phase nanotubes and the reference H-phase nanotubes are presented. For the considered diameter range, the lowest-energy T phase is found to be 1T'$_{AC}$ for AC nanotubes and 1T'$_{ZZ}$ for ZZ nanotubes, respectively, in WSe_2 system. As for $MoTe_2$ system, the 1T'' phase always stays as the lowest-energy T phase for all nanotubes. As seen in Figure 2, the energetically preferable phase changes from the T phase to the 2H phase as the nanotube diameter increases, indicating a T $\rightarrow$ 2H (or 2H $\rightarrow$ T) transition as the diameter increases (or decreases). Based on the calculated total energy, the effective strain energy $E_S^\phi(d)$, defined in Equation (1) above, can be obtained. The dependence of $E_S^\phi(d)$ on the diameter of the nanotube is shown in **Figure 3**. We can see that the 2H-phase nanotube always exhibits higher strain energy than that of the corresponding T-phase nanotube and the difference in the strain energy gradually diminishes as d increases. The critical diameter at which the transition occurs is denoted as d_c and the corresponding total energy is denoted as $E_{tube}^{critical}$. The values of d_c and $E_{tube}^{critical}$ are indicated in Figure 3 and also listed in **Table 1**.

The analysis of nanotube systems can serve as an important reference for mapping energy-deformation relation into a wider curvature space. From continuum mechanics, the strain energy of bending can be evaluated as

$$E_S^\phi(d) = \frac{1}{8} Y^\phi A_0^\phi \int_{-h^\phi/2}^{h^\phi/2} \frac{z^2}{d^2} dz = \frac{1}{96} Y^\phi A_0^\phi \frac{(h^\phi)^3}{d^2} = \frac{K^\phi}{d^2} \tag{2}$$

ADVANCED
SCIENCE NEWS

www.advancedsciencenews.com

ADVANCED
THEORY AND
SIMULATIONS

www.advtheorysimul.com

Figure 2. The normalized total energies (i.e., $E_{tube}^{\phi}(d)$) of the 2H phase and the lowest-energy T-phase nanotubes as functions of the diameter d, for a) AC nanotubes, and b) ZZ nanotubes of WSe$_2$, and c) AC nanotubes, and d) ZZ nanotubes of MoTe$_2$. The solid lines are from continuum prediction (see Equation (1)) while the discrete points are from DFT calculations.
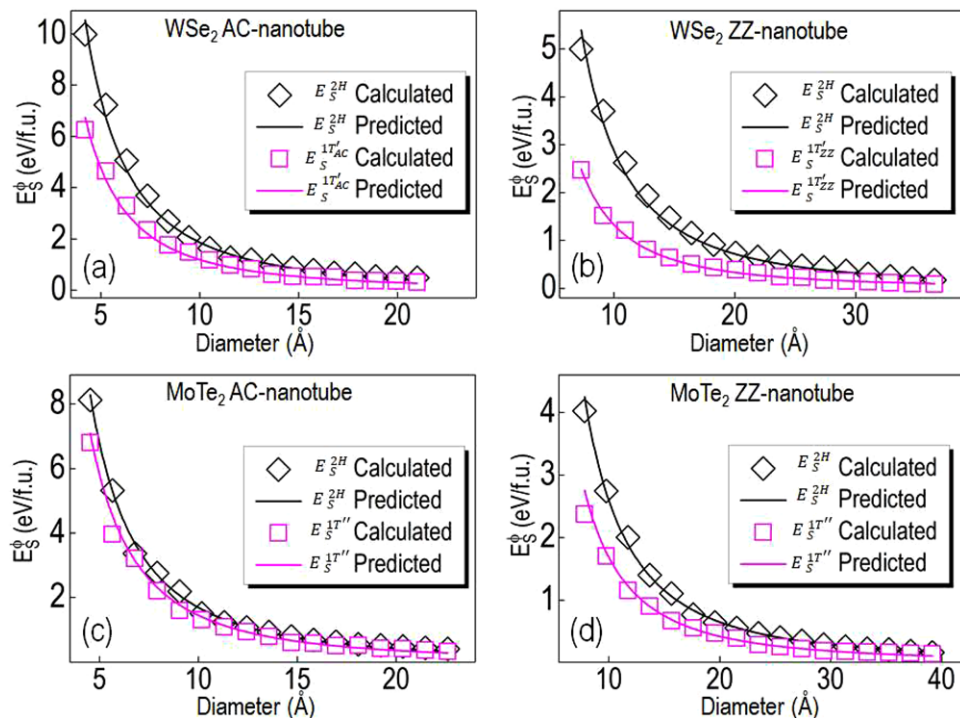
Figure 3. Comparison of calculated strain energy with continuum prediction for 2H phase and T phase with the lowest energy at the correspondent strain and phase conditions. The solid lines are from continuum prediction while the discrete points are from DFT calculations.

**ADVANCED
SCIENCE NEWS**

www.advancedsciencenews.com

**ADVANCED
THEORY AND
SIMULATIONS**

www.advtheorysimul.com

Table 1. Simulated and calculated parameters (d_c^{Sim}, d_c^{Pred}, K^ϕ, $E_{tube}^{critical}$) for curvature engineering. For each of the system, the bending directions (either armchair direction [AC] or zigzag direction [ZZ]) are indicated in the brackets. The simulated and calculated K^ϕ and $E_{tube}^{critical}$ are presented before and after slash, respectively.

System	WSe$_2$ (AC)	WSe$_2$ (ZZ)	MoTe$_2$ (AC)	MoTe$_2$ (ZZ)
d_c^{Sim} [Å]	14.71	23.72	18.09	29.37
d_c^{Pred} [Å]	14.28	21.64	17.86	31.85
Parameter	2H/T	2H/T	2H/T	2H/T
K^ϕ [eV · Å^2 f.u.$^{-1}$]	186.5/119.2	287.4/132.8	169.1/140.4	260.3/169.0
$E_{tube}^{critical}$ [eV f.u.$^{-1}$]	−21.69/−21.36	−21.69/−21.36	−18.03/−17.94	−18.03/−17.94

where Y^ϕ is Young's modulus for a specific phase ϕ, A_0^ϕ is the cross sectional area of phase ϕ, and h^ϕ is the effective thickness of phase ϕ. The constant $K^\phi = Y^\phi A_0^\phi (h^\phi)^3/96$ is the effective bending stiffness of material. By fitting Equation (2) to the data in Figure 3, the values of K^ϕ can be obtained, as tabulated in Table 1. We can see that the 2H phase always exhibits a higher bending stiffness than the T phase. Based on Equation (2), the difference in the strain energies stored in the 2H-phase and T-phase nanotubes can be determined:

$$\Delta E_S(d) = E_S^{2H}(d) - E_S^T(d) = \frac{(K^{2H} - K^T)}{d^2} \tag{3}$$

The phase transition observed in Figure 2 can be well explained by the competition between the strain and total energies. For both WSe$_2$ and MoTe$_2$, the 2H phase exhibits a lower total energy than the T phase, but a higher bending stiffness which causes a higher stain energy under bending deformation. In the case of a nanotube, the strain energy decreases as the diameter d increases (cf. Equation (2)), and consequently for large d, the total energy dominates and thus the 2H phase is preferred, while for small d, the strain energy prevails and thus the T phase becomes desirable. On the basis of the above competition, the critical diameter d_c corresponding to the transition can be predicted as:

$$d_c = \sqrt{\frac{K^{2H} - K^T}{E_{ml}^T - E_{ml}^{2H}}} \tag{4}$$

Plugging in the values of K^ϕ (see Table 1) into Equation (4), d_c can be obtained. As listed in Table 1, the predicted d_c shows an excellent agreement with the values determined from the DFT data.

As can be inferred from the analysis above, bending deformation will diminish the energy gap between the 2H and T phases. The above analysis may be further extended to more general bending deformation involving two perpendicular principle axes. Since Peierls distortion only occurs along the ZZ and AC directions of the TMD lattice to lead to the formation of lower-energy T phases (1T′ or 1T″), we consider the case where the ZZ and AC directions serve as the two bending directions. Assuming linear elasticity and superposition, the strain energy associated with the bending deformation will take the form:

$$E_S^\phi(d^{AC}, d^{ZZ}) = \frac{K^{\phi,AC}}{(d^{AC})^2} + \frac{K^{\phi,ZZ}}{(d^{ZZ})^2} \tag{5}$$

where the $K^{\phi,AC}$ and $K^{\phi,ZZ}$ refer to the effective bending stiffnesses determined from the nanotube model for the ϕ-phase AC nanotube and ZZ nanotube, respectively (see Figures 2 and 3 and Equation (2)). Denoting the critical diameters along the AC and ZZ directions in which the 2H → T phase transition occurs as (d_c^{AC}, d_c^{ZZ}), we have

$$\frac{K^{2H,AC} - K^{T,AC}}{(d^{AC})^2} + \frac{K^{2H,ZZ} - K^{T,ZZ}}{(d^{ZZ})^2} = E_{ml}^{2H} - E_{ml}^T \tag{6}$$
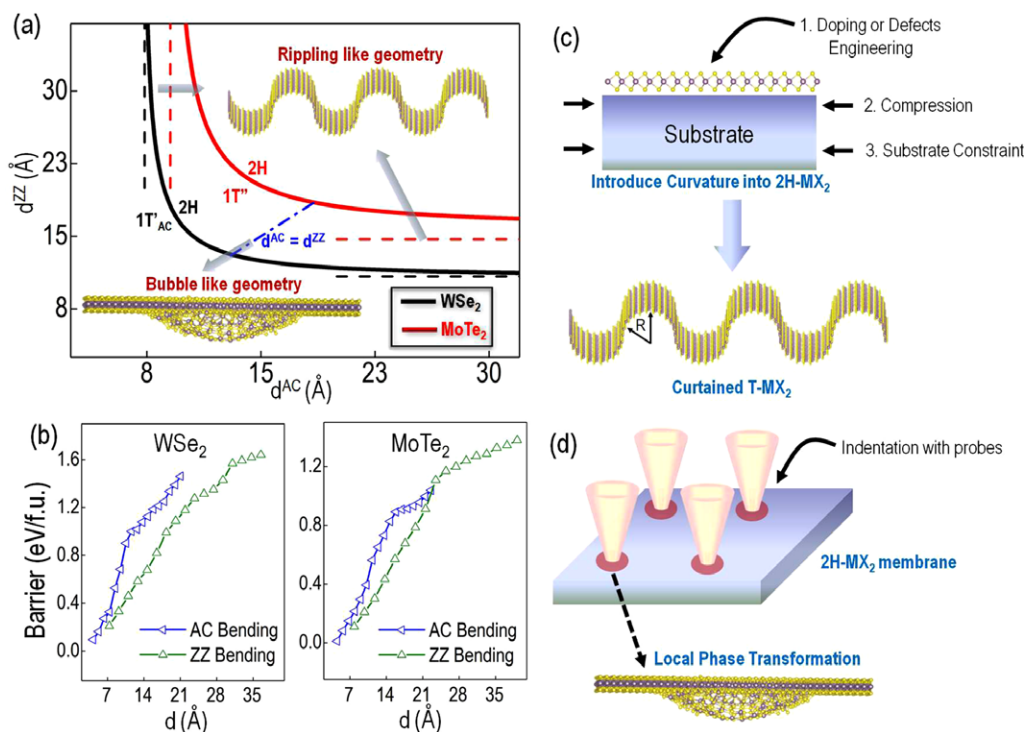
From the above equation, the phase stability diagram for a TMD material under bidirectional bending deformation can be obtained, as demonstrated in **Figure 4**a.

With the coexistence of two principle bending axes, two types of deformation can be conveniently introduced in the experiment, which are indicated in Figure 4a with dotted lines and dotted dashed lines. To be more specific, when the bending diameter in 1D approaches infinity, the TMD membrane will experience a rippling-like deformation. The critical diameter for phase transition can be obtained from the asymptotes of the corresponding phase boundaries as shown in Figure 4a. On the other hand, when there are comparable amounts of bending deformation in both AC and ZZ direction, the membrane will undergo bubble-like deformation, which is illustrated in Figure 4a with the dot dash line.

Meanwhile, to further confirm the feasibility of the route of curvature engineering in inducing phase transition, we studied the kinetics of phase transition using transition state theory.[46,49] The evolution of activation barrier under single axis bending deformation is demonstrated in Figure 4b for WSe$_2$ and MoTe$_2$. It can be inferred from Figure 4b that with the decreasing of bending diameter, the activation barrier will decrease monotonically. More specifically, when bending deformation is at critical diameter as shown in Table 1, the activation barriers required are reduced from more than 1.6 eV f.u.$^{-1}$ and 1.3 eV f.u.$^{-1}$ in WSe$_2$ monolayer into around 1.1 eV f.u.$^{-1}$ and 1.0 eV f.u.$^{-1}$ at phase transition critical diameter. This trend implicates that large bending information will also enhance the kinetic procedure due to the dropping of the phase transition barrier.

In the experiment, the rippling-like geometry can be introduced from doping,[50] defect engineering,[47,51] compressive mechanical deformation,[52] or substrate constraint,[53,54] as demonstrated by the schematic design in Figure 4c. When the deformation is large enough to create bending diameter that is less than the critical one as predicted in Figure 4a, structural

ADVANCED
SCIENCE NEWS
www.advancedsciencenews.com

ADVANCED
THEORY AND
SIMULATIONS
www.advtheorysimul.com

Figure 4. a) The phase stability diagram taking zigzag and armchair directions as the bending principle axes. The phase transition boundary from 2H phase into T phase with the lowest energy is visualized. We use red line to show the phase boundary of WSe$_2$ and black line to show the phase boundary of MoTe$_2$, b) activation barriers with different amount of single axis bending diameters for WSe$_2$ and MoTe$_2$, c) schematic illustration of potential designs of introducing rippling to induce 2H $\rightarrow$ T (1T′, 1T″) phase transition in TMDs, and d) schematic illustration of programmable local 2H $\rightarrow$ T (1T′, 1T″) phase transition in TMDs with indentation from probes.

phase transition will happen. Even with the release of elastic strain, the T phases will last due to the relatively large barrier to transform from T phases back to the 2H phase.[32,33] On the other hand, bubble-like deformation can be created by nanoindentation using nanometer size probe as demonstrated by the schematic design in Figure 4d.[55,56] With the controlling of indentation site, localized curvature can be introduced into 2H-TMD membrane, which will result in localized domains transforming into T phases. With a patterned indentation, the local T regions can be programmed so that various patterns of T phases can be printed in to 2H-TMD membrane. Due to the extinguish electronic and optical properties provided by 2H and T phases of TMD,[27,32,35,50] various novel heterostructures and nanodevice, such as quantum dots of T phases planted in 2H-TMD,[50] low resistance planar 2H/T heterostructures[32] could be directly architected from nanoindentation techniques.

The possibility of tuning phase stability within TMDs through curvature engineering was investigated combining first-principles calculations and continuum mechanics analysis. It has been determined that with bending deformation, 2H $\rightarrow$ T phase transition would be rendered energetically favorable as well as kinetically facilitated. Meanwhile, phase stability diagram has been constructed which indicates that different degrees of phase transformation can be tailored by varying the amount of deformation in two perpendicular bending axes. Specifically, rippling would be an effective way to introduce uniformly phase transformation while bubble-like deformation can be applied in precisely pat-

terning of local T domains on the 2H-TMD membranes. Our theoretical results not only provide a feasible way to manipulate structural phase of 2H-TMDs using mechanical deformation, but also sheds light on simplified design and fabrication of novel heterostructures and nanodevices.

Conflict of Interest

The authors declare no conflict of interest.

**ADVANCED
SCIENCE NEWS**

www.advancedsciencenews.com

**ADVANCED
THEORY AND
SIMULATIONS**

www.advtheorysimul.com

[1] S. Butun, S. Tongay, K. Aydin, *Nano Lett.* **2015**, *15*, 2700.

[2] W. Wu, L. Wang, Y. Li, F. Zhang, L. Lin, S. Niu, D. Chenet, X. Zhang, Y. Hao, T. F. Heinz, J. Hone, Z. L. Wang, *Nature* **2014**, *514*, 470.

[3] E. J. Reed, *Nat. Nano.* **2015**, *10*, 106.

[4] H. Zhu, Y. Wang, J. Xiao, M. Liu, S. Xiong, Z. J. Wong, Z. Ye, Y. Ye, X. Yin, X. Zhang, *Nat. Nano.* **2015**, *10*, 151.

[5] T. Wu, H. Zhang, *Angew. Chem. Int. Ed. Engl.* **2015**, *54*, 4432.

[6] K. He, N. Kumar, L. Zhao, Z. Wang, K. F. Mak, H. Zhao, J. Shan, *Phys. Rev. Lett.* **2014**, *113*, 026803.

[7] K. F. Mak, K. L. McGill, J. Park, P. L. McEuen, *Science* **2014**, *344*, 1489.

[8] M. Bernardi, M. Palummo, J. C. Grossman, *Nano Lett.* **2013**, *13*, 3664.

[9] M. Wu, X. Qian, J. Li, *Nano Lett.* **2014**, *14*, 5350.

[10] J. Feng, X. Qian, C.-W. Huang, J. Li, *Nat. Photon.* **2012**, *6*, 866.

[11] O. Lopez-Sanchez, E. Alarcon Llado, V. Koman, A. Fontcuberta i Morral, A. Radenovic, A. Kis, *ACS Nano* **2014**, *8*, 3042.

[12] M.-L. Tsai, S.-H. Su, J.-K. Chang, D.-S. Tsai, C.-H. Chen, C.-I. Wu, L.-J. Li, L.-J. Chen, J.-H. He, *ACS Nano* **2014**, *8*, 8317.

[13] Y. J. Zhang, J. T. Ye, Y. Yomogida, T. Takenobu, Y. Iwasa, *Nano Lett.* **2013**, *13*, 3023.

[14] C.-H. Lee, G.-H. Lee, A. M. van der Zande, W. Chen, Y. Li, M. Han, X. Cui, G. Arefe, C. Nuckolls, T. F. Heinz, J. Guo, J. Hone, P. Kim, *Nat. Nano.* **2014**, *9*, 676.

[15] S. Tongay, J. Suh, C. Ataca, W. Fan, A. Luce, J. S. Kang, J. Liu, C. Ko, R. Raghunathanan, J. Zhou, F. Ogletree, J. Li, J. C. Grossman, J. Wu, *Sci. Rep.* **2013**, *3*, https://doi.org/10.1038/srep02657.

[16] K. Roy, M. Padmanabhan, S. Goswami, T. P. Sai, G. Ramalingam, S. Raghavan, A. Ghosh, *Nat. Nano.* **2013**, *8*, 826.

[17] R. S. Sundaram, M. Engel, A. Lombardo, R. Krupke, A. C. Ferrari, P. Avouris, M. Steiner, *Nano Lett.* **2013**, *13*, 1416.

[18] W. Li, J. Li, *Nat. Commun.* **2016**, *7*, https://doi.org/10.1038/ncomms8381.

[19] K.-A. N. Duerloo, Y. Li, E. J. Reed, *Nat. Commun.* **2014**, *5*, 4214.

[20] B. Ouyang, G. Lan, Y. Guo, Z. Mi, J. Song, *Appl. Phys. Lett.* **2015**, *107*, 191903.

[21] B. Ouyang, P. Ou, Y. Wang, Z. Mi, J. Song, *Phys. Chem. Chem. Phys.* **2016**, *18*, 33351.

[22] A. Ambrosi, Z. Sofer, M. Pumera, *Chem. Comm.* **2015**, *51*, 8450.

[23] M. A. Lukowski, A. S. Daniel, F. Meng, A. Forticaux, L. Li, S. Jin, *J. Am. Chem. Soc* **2013**, *135*, 10274.

[24] X. Geng, W. Sun, W. Wu, B. Chen, A. Al-Hilo, M. Benamara, H. Zhu, F. Watanabe, J. Cui, T.-P. Chen, *Nat. Commun.* **2016**, *7*, 10672.

[25] M. Mortazavi, C. Wang, J. Deng, V. B. Shenoy, N. V. Medhekar, *J. Power Sources* **2014**, *268*, 279.

[26] M. Acerce, D. Voiry, M. Chhowalla, *Nat. Nano.* **2015**, *10*, 313.

[27] X. Qian, J. Liu, L. Fu, J. Li, *Science* **2014**, *346*, 1344.

[28] D. H. Keum, S. Cho, J. H. Kim, D.-H. Choe, H.-J. Sung, M. Kan, H. Kang, J.-Y. Hwang, S. W. Kim, H. Yang, K. J. Chang, Y. H. Lee, *Nat. Phys.* **2015**, *11*, 482.

[29] D.-H. Choe, H.-J. Sung, K. J. Chang, *Phys. Rev. B* **2016**, *93*, 125109.

[30] L. Liu, J. Guo, *J. Appl. Phys.* **2015**, *118*, 124502.

[31] J. J. Cha, K. J. Koski, Y. Cui, *Phys. Status Solidi* **2013**, *7*, 15.

[32] R. Kappera, D. Voiry, S. E. Yalcin, B. Branch, G. Gupta, A. D. Mohite, M. Chhowalla, *Nat. Mater.* **2014**, *13*, 1128.

[33] Y. Guo, D. Sun, B. Ouyang, A. Raja, J. Song, T. F. Heinz, L. E. Brus, *Nano Lett.* **2015**, *15*, 5081.

[34] C. Mai, A. Barrette, Y. Yu, Y. G. Semenov, K. W. Kim, L. Cao, K. Gundogdu, *Nano Lett.* **2014**, *14*, 202.

[35] B. Ouyang, Z. Mi, J. Song, *J. Phys. Chem. C* **2016**, *120*, 8927.

[36] S. Bertolazzi, J. Brivio, A. Kis, *ACS Nano* **2011**, *5*, 9703.

[37] B. Ouyang, S. Xiong, Z. Yang, Y. Jing, Y. Wang, *Nanoscale* **2017**, *9*, 8126.

[38] S. Xiong, G. Cao, *Nanotechnology* **2016**, *27*, 105701.

[39] X. Liu, D. Pan, Y. Hong, W. Guo, *Phys. Rev. Lett.* **2014**, *112*, 205502.

[40] L. Yu, A. Ruzsinszky, J. P. Perdew, *Nano Lett.* **2016**, *16*, 2444.

[41] Y. Wei, B. Wang, J. Wu, R. Yang, M. L. Dunn, *Nano Lett.* **2013**, *13*, 26.

[42] I. Nikiforov, E. Dontsova, R. D. James, T. Dumitrică, *Phys. Rev. B* **2014**, *89*, 155437.

[43] A. P. Nayak, T. Pandey, D. Voiry, J. Liu, S. T. Moran, A. Sharma, C. Tan, C.-H. Chen, L.-J. Li, M. Chhowalla, J.-F. Lin, A. K. Singh, D. Akinwande, *Nano Lett.* **2014**, *15*, 346.

[44] G. Kresse, J. Furthmüller, *Phys. Rev. B* **1996**, *54*, 11169.

[45] P. Hohenberg, W. Kohn, *Phys. Rev.* **1964**, *136*, B864.

[46] D. Sheppard, R. Terrell, G. Henkelman, *J. Chem. Phys* **2008**, *128*, 134106.

[47] G. Henkelman, B. P. Uberuaga, H. Jónsson, *J. Chem. Phys* **2000**, *113*, 9901.

[48] R. A. Olsen, G. J. Kroes, G. Henkelman, A. Arnaldsson, H. Jónsson, *J. Chem. Phys* **2004**, *121*, 9776.

[49] J. P. Perdew, K. Burke, M. Ernzerhof, *Phys. Rev. Lett.* **1996**, *77*, 3865.

[50] Y.-C. Lin, D. O. Dumcenco, Y.-S. Huang, K. Suenaga, *Nat. Nano.* **2014**, *9*, 391.

[51] A. Kushima, X. Qian, P. Zhao, S. Zhang, J. Li, *Nano Lett.* **2015**, *15*, 1302.

[52] S. Deng, V. Berry, *Mater. Today* **2016**, *19*, 197.

[53] D. Nandwana, E. Ertekin, *Nano Lett.* **2015**, *15*, 1468.

[54] D. Nandwana, E. Ertekin, *J. Appl. Phys.* **2015**, *117*, 234304.

[55] J. Berry, S. Zhou, J. Han, D. J. Srolovitz, M. P. Haataja, *Nano Lett.* **2017**, *17*, 2473.

[56] S. Manzeli, A. Allain, A. Ghadimi, A. Kis, *Nano Lett.* **2015**, *15*, 5330.